

## **Sensorless speed observer for industrial drives based induction motors with low complexity**

Dabour, Sherif; Hussien, Mohamed ; Aboushady, Ahmed; Farrag, Mohamed E.

*Published in:*

Induction Motors - Recent Advances, New Perspectives and Applications

*DOI:*

[10.5772/intechopen.1001150](https://doi.org/10.5772/intechopen.1001150)

*Publication date:*

2023

*Document Version*

Publisher's PDF, also known as Version of record

[Link to publication in ResearchOnline](#)

*Citation for published version (Harvard):*

Dabour, S, Hussien, M, Aboushady, A & Farrag, ME 2023, Sensorless speed observer for industrial drives based induction motors with low complexity. in A El-Shahat (ed.), *Induction Motors - Recent Advances, New Perspectives and Applications*. IntechOpen. <https://doi.org/10.5772/intechopen.1001150>

### **General rights**

Copyright and moral rights for the publications made accessible in the public portal are retained by the authors and/or other copyright owners and it is a condition of accessing publications that users recognise and abide by the legal requirements associated with these rights.

### **Take down policy**

If you believe that this document breaches copyright please view our takedown policy at <https://edshare.gcu.ac.uk/id/eprint/5179> for details of how to contact us.

# We are IntechOpen, the world's leading publisher of Open Access books Built by scientists, for scientists

6,300

Open access books available

172,000

International authors and editors

190M

Downloads

Our authors are among the

154

Countries delivered to

TOP 1%

most cited scientists

12.2%

Contributors from top 500 universities



WEB OF SCIENCE™

Selection of our books indexed in the Book Citation Index  
in Web of Science™ Core Collection (BKCI)

Interested in publishing with us?  
Contact [book.department@intechopen.com](mailto:book.department@intechopen.com)

Numbers displayed above are based on latest data collected.  
For more information visit [www.intechopen.com](http://www.intechopen.com)



## Chapter

# Sensorless Speed Observer for Industrial Drives Based Induction Motors with Low Complexity

*Sherif Dabour, Mohamed Hussien, Ahmed Aboushady and Mohamed E. Farrag*

## Abstract

This chapter presents a simple method to efficiently predict the rotor speed for a sensorless vector control technique applied to induction motors (IMs). The motor is supplied by a Simplified Split-Source Inverter (S<sup>3</sup>I), which provides dc-boosting and ac-inversion processes during input voltage sag. It also has a wider modulation range and a lower harmonic content than conventional boosting inverters. With this contribution, it is possible to efficiently estimate the rotor position directly without needing a PI controller with fluctuated supply voltage. The proposed strategy can be divided into three parts. The first uses a dual-loop controller to obtain the reference DC-boosted voltage of the SSI and regulate the input current. The second is the suggested observer for speed detection, which is derived from the principles of phase axis relations of the adopted machine currents and the indirect rotor flux orientation control (IRFOC) approach. With a newly developed space vector modulation, the third part will generate the switching pulses of the inverter switches. A complete analysis has been conducted to ensure the observability of the proposed technique. A series of PLECS simulations were conducted to verify the concept. The obtained results validate the proposed strategy with the S<sup>3</sup>I topology.

**Keywords:** induction motor, split-source inverter, sensorless observer for speed detection, vector control technique

## 1. Introduction

Due to their low cost, high power density, and ability to withstand harsh environments, induction motors are the most popular motors in the industry [1, 2]. If this motor is directly connected to the grid, it operates at speeds determined by the line frequency and the number of poles. Due to the nonlinear relationship between motor current and torque, speed control is much more complex than DC motors. During the past few years, there have been numerous applications for induction motors, including pumps, blowers, and industrial applications. Although this control strategy is easy to implement and utilizes inexpensive hardware, it has poor performance and slow response times. Nevertheless, modern variable speed drive applications, such as

electric vehicles (EVs), require high performance and fast dynamic response control systems.

To improve the dynamic responses of the electric drive systems, vector control strategies, such as the Field-oriented Control (FOC) method, are proposed [3–5]. According to this control method, flux is controlled by the amount of current generated on the d-axis, while the current component on the q-axis controls torque. Based on this approach, the induction motor mimics the dynamic behavior of a DC motor. The advantages of FOC include a wider speed range, better dynamic response, precise speed and position control, and field weakening (movement beyond base speed). In this control method, it is possible to directly measure the position of the field or the motor speed using the hall effect sensor. However, this method increases the system cost and the need for maintenance.

Low-cost and highly reliable controlled IM drives without mechanical sensors at the motor shaft have been demonstrated in the literature. It's called sensorless vector control algorithms. In these algorithms, to replace the sensor, the stator voltages and currents at the motor terminals are measured to determine the rotor speed or position [3–5]. The dynamic equations of induction motors can be used to estimate several quantities, such as magnetic flux and frequency. However, these quantities often require expensive or difficult-to-implement physical sensors. This class only requires current and voltage sensors. Accurate knowledge of machine parameters and open equations for estimates is necessary. On the other hand, closed-loop observatories rely on flexible techniques that require more computational power [6–18].

In general, a conventional voltage source inverter (VSI) can only achieve an output voltage that is limited by the input voltage level of the DC supply [19, 20]. Therefore, the new topology overcomes the performance-enhancing potential of DC-AC power converters, such as the Z-Source Topology Converter (ZSI). However, there are some issues, such as the lack of input current continuity and the use of four passive elements. Therefore, S<sup>3</sup>I (Simplified Split Source Inverter) topology can be used instead of ZSI, as shown in **Figure 1**, which handles the benefits of continuous input current and the reduced need for passive components [21]. Due to their advantages, the SSI is recently considered in different applications and control techniques, such as model predictive control [22], virtual synchronous control [23], dual motor drive [24], multilevel converter topologies [25] and multiphase machine drives [26].

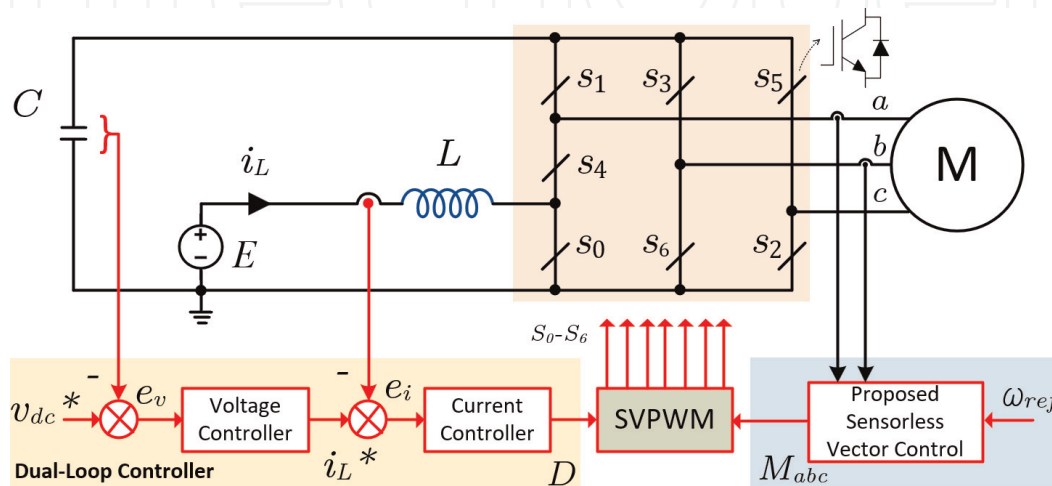


**Figure 1.** Simplified Split-source inverter feeding three-phase induction motor.

This chapter aims to present a simple method for efficiently predicting the induction motor speed, which is supplied by S<sup>3</sup>I directly without a speed sensor. Basically, there are three parts to the control strategy. In the first part, the dc-link voltage  $v_{dc}$  and the supply current  $i_L$ , shown in **Figure 1**, are controlled by a dual-loop controller. In the second part, we propose a new speed observer derived from the principles of phase axis relationships of the adopted machine currents and indirect rotor flux orientation control (IRFOC). The third part will be used to generate the gating pulses of S<sup>3</sup>I with a modified SVPWM approach. Finally, the concept behind this chapter was verified using simulations.

## 2. Dynamic model of IM

The voltage and current relations for three-phase IM in the  $dq$ -axes are described as follows:

$$\begin{cases} v_{q_s} = r_s i_{q_s} + \frac{d}{dt} \lambda_{q_s} + \omega \lambda_{d_s} \\ v_{d_s} = r_s i_{d_s} + \frac{d}{dt} \lambda_{d_s} - \omega \lambda_{q_s} \\ 0 = r_r i_{q_r} + \frac{d}{dt} \lambda_{q_r} + (\omega - \omega_r) \lambda_{d_r} \\ 0 = r_r i_{d_r} + \frac{d}{dt} \lambda_{d_r} - (\omega - \omega_r) \lambda_{q_r} \end{cases} \quad v_{q_s} = r_s i_{q_s} + \frac{d\lambda_{q_s}}{dt} + \omega \lambda_{d_s} \quad (1)$$

where,

$$\begin{cases} \omega = \frac{P}{2} \omega_f \\ \omega_r = \frac{P}{2} \omega_{rm} \end{cases} \quad (2)$$

The associated relations of flux linkage are given as follows

$$\begin{cases} \lambda_{q_s} = L_s i_{q_s} + L_m i_{q_r} \\ \lambda_{d_s} = L_s i_{d_s} + L_m i_{d_r} \\ \lambda_{q_r} = L_r i_{q_r} + L_m i_{q_s} \\ \lambda_{d_r} = L_r i_{d_r} + L_m i_{d_s} \end{cases} \quad (3)$$

where,

$$\begin{cases} L_s = L_{ls} + L_m \\ L_r = L_{lr} + L_m \end{cases} \quad (4)$$

The corresponding electromagnetic torque can be obtained as follows

$$T_e = \left(\frac{3}{2}\right) \left(\frac{P}{2}\right) \left(\frac{L_m}{L_r}\right) (\lambda_{d_r} i_{q_s} - \lambda_{q_r} i_{d_s}) \quad (5)$$

Furthermore, the overall torque expression can be realized by

$$T_e = T_L + J \frac{d\omega_{rm}}{dt} + B \omega_{rm} \quad (6)$$

### 3. Proposed sensorless vector-control strategy

In general, vector control strategies are classified into direct field-oriented control (DFOC) and indirect field-oriented control (IRFOC) [3–5]. This chapter concerns the IRFOC technique. According to the field orientation principle of the three-phase IM, the magnetic flux and motor torque can be controlled independently by injecting appropriate stator currents or voltages [4]. The dynamic equations of the three-phase IM, which are presented by (1)–(6), can be simplified under certain conditions. For rotor-driven control, the rotor flux is aligned with the excitation frame ( $\lambda_{dr} = \lambda_r$ ) and the expression is simplified so that  $\lambda_{qr}$  equals zero ( $\lambda_{qr} = 0$ ). Since the resulting motor's torque and flux are decoupled. In this way, the IM can be controlled like a DC motor [2]. In this technique, the synchronous speed required to maintain the orthogonal orientation of vectors  $\lambda_r$  and  $i_r$  in field-oriented control (FOC) is denoted by  $\omega_e^*$ . For the proposed orientation of the rotor winding field, the IM phase-axis relationship is shown in **Figure 2**.

The required slip speed  $\omega_r$  and the desired current  $i_s^*$  to produce the torque  $T_e^*$  and the desired magnetic flux  $\lambda_r^*$  are calculated from the motor equations and the orientation conditions of the magnetic field. Manipulating the equilibrium equations, we obtain the following equation, which represents an indirect vector controller:

$$i_{q_s}^* = \left(\frac{2}{3}\right) \left(\frac{2}{P}\right) \left(\frac{L_r}{L_m}\right) \frac{T_e^*}{\lambda_r} \quad (7)$$

$$i_{d_s}^* = \frac{\lambda_r^*}{L_m} \quad (8)$$

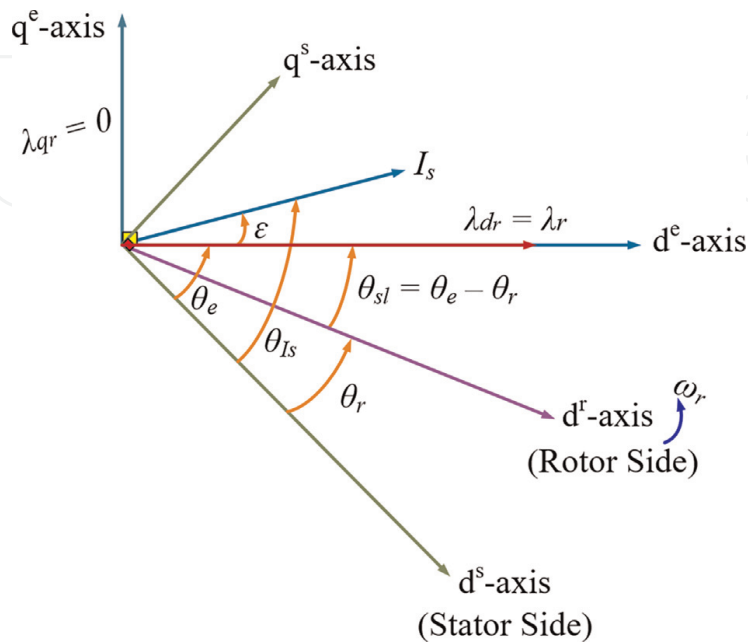


**Figure 2.** Phase-axis relationship of the IM for the proposed control strategy.

Furthermore, the angular reference speed  $\omega_e^*$  can be obtained from the machine rotor speed  $\omega_r$ , and the slip speed  $\omega_{sl}$  as follows

$$\omega_e^* = \omega_{sl} + \omega_r \quad (9)$$

Note that the relevant frame angle  $\theta_e$  can be found directly by integrating  $\omega_e^*$ . In the indirect FOC (IRFOC) technique, the slip speed,  $\omega_{sl}$  is determined from [2], as follows

$$\omega_{sl} = \frac{L_m r_r}{\lambda_r L_r} \dot{i}_{q_s} \quad (10)$$

Based on the principles of the introduced IRFOC, the real flux of the rotor  $\lambda_r$  is calculated as:

$$\frac{L_r}{r_r} \frac{d\lambda_r}{dt} + \lambda_r = L_m i_{d_s} \quad (11)$$

The stator current component corresponding to the  $dq$ -axis can be determined from the actual three-phase currents using the desired frame angle (frame angle,  $\theta_f = \theta_e$ ) with a suitable conversion (given  $K_{tr}$ ):

$$K_{tr} = \frac{2}{3} \begin{bmatrix} \cos \theta_f & \cos \left( \theta_f - \frac{2\pi}{3} \right) & \cos \left( \theta_f + \frac{2\pi}{3} \right) \\ -\sin \theta_f & -\sin \left( \theta_f - \frac{2\pi}{3} \right) & -\sin \left( \theta_f + \frac{2\pi}{3} \right) \end{bmatrix} \quad (12)$$

It is worth noting that the vector control algorithm for the desired orientation depends on the rotor speed signal. However, the necessary speed sensor increases the overall system cost and requires more maintenance. Therefore, it is recommended to implement speed control based magnetic field orientation using a more efficient sensorless rotor speed monitor. Therefore, this section explores a simple method to detect the speed of the IM without an additional observer. The block diagram of the proposed sensorless control strategy is shown in **Figure 3**. The main control procedure applied can be illustrated as follows:

First, the phase angle,  $\theta_{I_s}$  and the current space vector of the stator side,  $i_s$  are determined from the actual three-phase signals as follows

$$\begin{cases} i_s = k \cdot i_{abc_s} \\ \theta_{I_s} = \text{angle} ( i_s ) \end{cases} \quad (13)$$

where  $k = \left( \frac{2}{3} \quad \frac{2}{3}e^{j\frac{2\pi}{3}} \quad \frac{2}{3}e^{j\frac{4\pi}{3}} \right)$

In addition, the slip angle  $\theta_{sl}$  can be obtained directly from the relevant slip angle velocity integration process using (10). Therefore, the corresponding amount of the expected rotor current on the  $dq$  axis is given using a transformation matrix, where  $K_{tr}$  is the angle of the indicated magnetic flux direction ( $\theta_f = \theta_{sl}$ ).

Then, the corresponding shaft stator current  $dq$  can be determined using the IRFOC ( $\lambda_{q_r} = 0$ ) in (3) and (11). Therefore, the relevant phase angle is expressed as







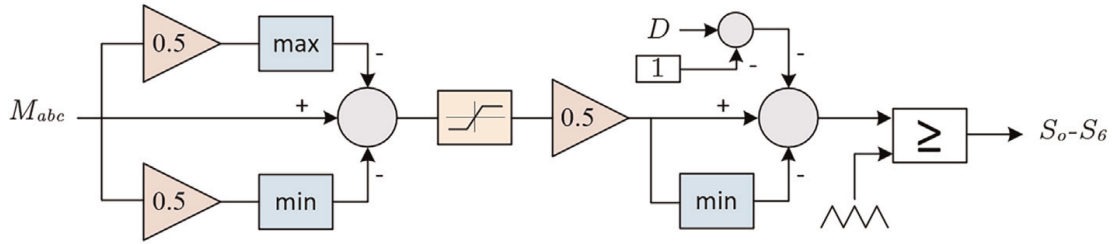


**Figure 4.** Block diagram for generating the gating pulses using the proposed SVPWM approach for the  $S^3I$ .

By adjusting the rotor flux,  $\lambda_r^*$  and the electromagnetic torque,  $T_e^*$  we can obtain the command values of the stator current  $i_{d_s}^*$  and  $i_{q_s}^*$  can be obtained in the expected frame  $dq$  as shown in **Figure 3**. Therefore, the corresponding three-phase stator current can be specified using the transformation matrix  $K_{tr}$  along with the desired frame angle  $\theta_e$ .

The three-phase modulating signals,  $M_{abc}$  are determined using Synchronous Current Control (SSC) technique, as shown in **Figure 3**. In SCC, two pairs of current controllers are used to evaluate reference voltages in the synchronous reference frame. After these voltages have been converted to three-phase, they are utilized as references for modulation.

Finally, the SVPWM modulator handles the signals from the dual-loop controller and the sensorless controller to obtain the gating pulses of the inverter, as shown in **Figure 4** [31].

It is worth noting the dc boosting factor,  $B$  of the analyzed inverter circuit ( $B$  is defined as the ratio between the capacitor average voltage and the supply voltage) and can be calculated from the charging duty cycle,  $D$ , which is determined from the dual-loop controller for the dc-side and is governed by [31].

$$B = \frac{1}{1 - D} \quad (18)$$

Moreover, the voltage gain, which is defined as the ratio between the peak value of the phase voltage to the supply voltage, is [31].

$$G = \frac{M}{2 \sin(2\pi/3)(1 - D)} \quad (19)$$

#### 4. Simulation study

Simulation models have been developed using PLECS© software for the proposed sensorless control technique of a three-phase induction motor drive fed by  $S^3I$ . The system and motor parameters are listed in **Tables 1** and **2**. The induction motor was simulated using  $dq$ -model in the stationary reference frame, and the dc- and ac-sides were controlled using the proposed strategy with the given parameters. The reference torque is limited to the motor-rated torque (3.75 Nm). Forced excitation is initiated before powering up the drive system to keep the rotor flux at the rated value for speed lower than the base value. Therefore, at the time of speed reference application, the rotor flux is

Parameter	Value	Parameter	Value
Power [kW]	2	Rs [ $\Omega$ ]	4.2
Line voltage [V]	380 V	Rr [ $\Omega$ ]	4.37
No. of poles	2-pole	Ls [H]	0.8714
Frequency [Hz]	50 Hz	Lr [H]	0.8714
Inertia	0.03	Lm [H]	0.85

**Table 1.**  
Parameters of the three-phase induction machine.

Parameter	Value	Parameter	Value
Torque limit	3.75	DC voltage controller	$k_p$ 0.5
Initial rotor flux	1.525		$k_i$ 0.04
Speed controller	$k_p$ 2.67	DC current controller	$k_p$ 1
	$k_i$ 118.5		$k_i$ 0.5

**Table 2.**  
Parameters and gains for Sensorless and dual-loop controller.

previously stabilized at the rated value. To verify the validity of the PLECS models developed for the proposed drive system, a series of simulation results have been obtained for supply voltage dip, acceleration, a step change in speed, disturbance rejection, and speed reversal transients. The results shown in **Figures 5–10** have been classified into two case studies: 1) supply voltage dip and 2) constant supply voltage case (**Table 2**).

#### 4.1 Supply voltage dip

In this case, it is assumed that the supply voltage is 300 V for the first 1.3 sec of the simulation. Afterwards, it was reduced to 150 for 0.4 sec and then restored to its original value. Moreover, the motor is accelerated at  $t = 0.3$  sec from the standstill to 1000 rpm at no-load in 0.7 seconds. After that, a load of 1.5 Nm is applied at  $t = 1$  sec.

The waveforms of supply voltage, charging duty cycle, dc-link voltage and motor terminal voltage are shown in **Figure 5**. Moreover, **Figures 6** and **7** show the actual and reference  $dq$  components of the motor current; the motor reference and estimated speed; the reference and actual motor torque; and actual phase currents waveforms, respectively, for the case study. It can be observed from these results that:

It can be observed from **Figure 5** that

- The proposed topology initially boosts the supply voltage from 300 to 600 volts at the dc-link capacitor.
- Furthermore, the dual loop controller can follow the reference dc-link voltage and the inductor current references despite disturbances with small ripples.
- The duty cycle,  $D$  is changed during the voltage dip period to obtain a constant dc-link capacitor voltage at the capacitor terminal (600 V) and, therefore, the required voltage at the motor terminals.

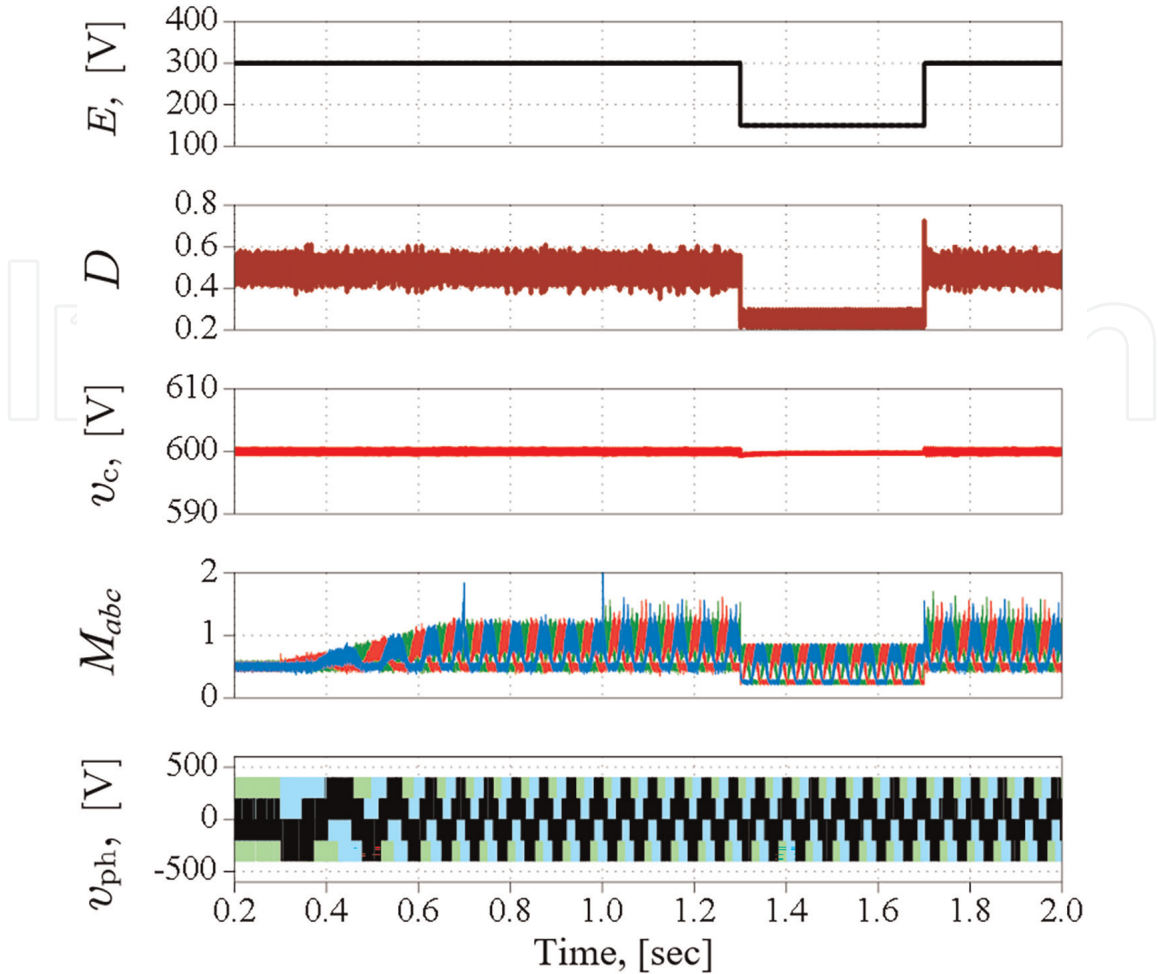


**Figure 5.** Simulation results for the supply voltage, charging duty cycle, capacitor voltage, modulating signals and motor phase voltages, respectively, of the suggested sensorless control strategy of the proposed system for voltage dip from 300 V to 150 V.

- The motor currents' actual flux and torque components are fully decoupled and follow the reference components generated from the IFOC very well.
- The motor runs from the standstill to 1000 rpm in about 0.4 sec, and the motor torque follows the reference torque with a fast response.
- An accurate motor speed estimation is achieved from the simulation results of the proposed algorithm.
- In addition, the motor currents have sinusoidal waveforms with a THD of less than 3.4%.

#### 4.2 Constant supply voltage

In this case, the supply voltage is assumed to be a constant of 300 V. An acceleration with ramp change from 0 to 1000 rpm at no-load during the interval from  $t = 0.3$  to  $t = 1$  second, then a load of 1.5 Nm is applied from  $t = 1$  to  $t = 1.6$  sec. After that, speed reversal during the interval from  $t = 2$  to  $t = 2.8$  sec is applied to 1000 rpm in

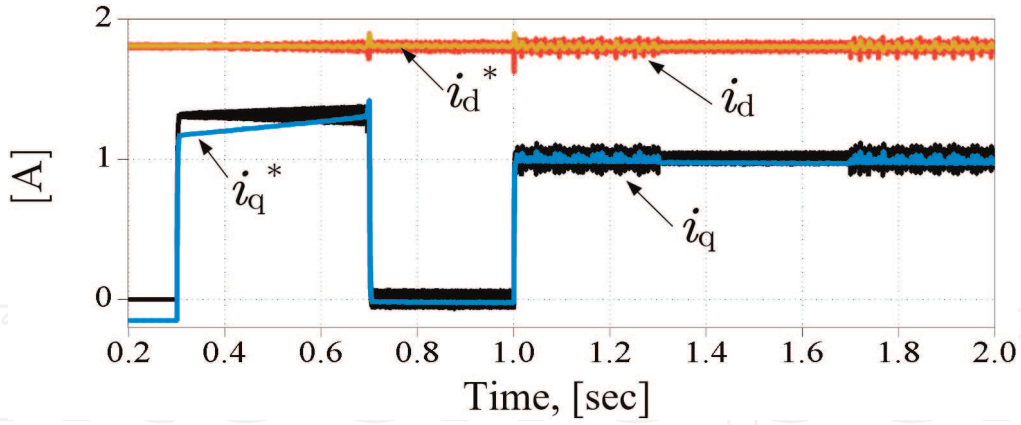


**Figure 6.** Simulation results for the reference and actual motor current dq-axes components of the suggested sensorless control strategy of the proposed system for voltage dip from 300 V to 150 V.

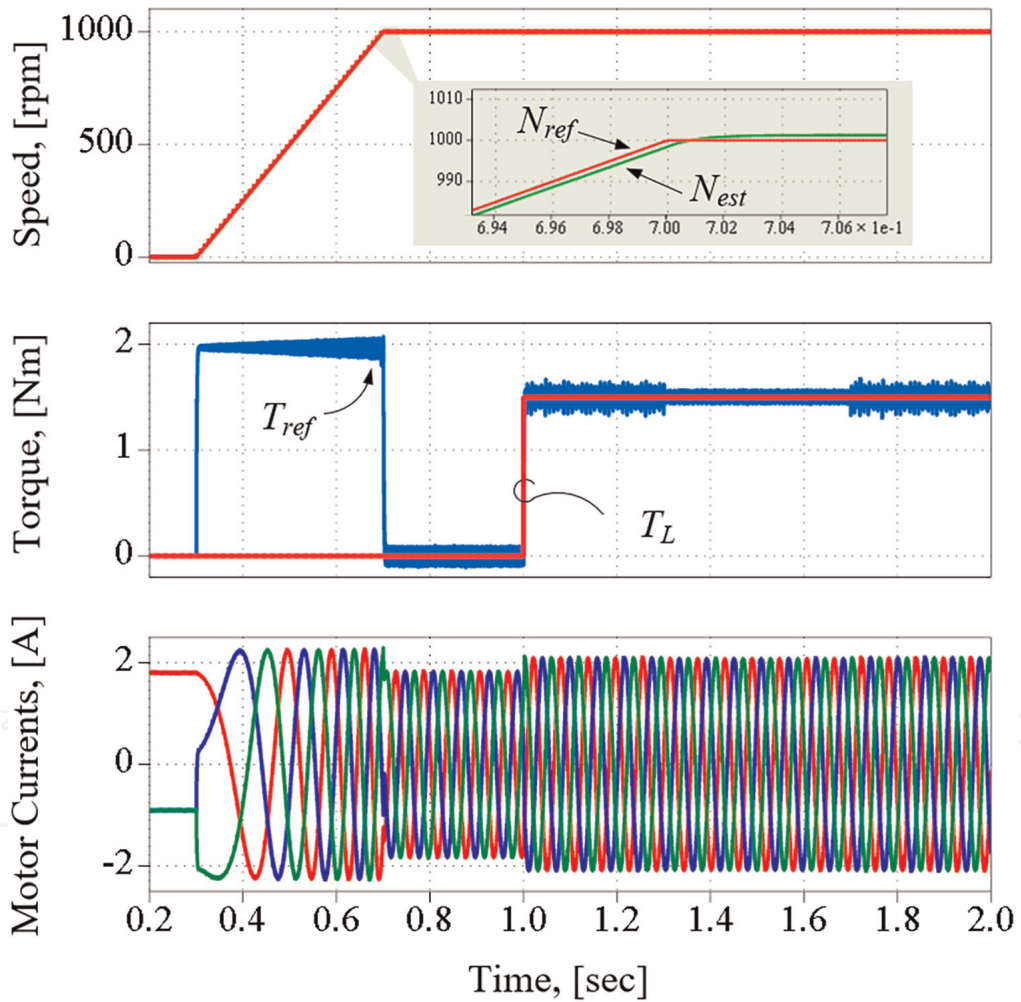


**Figure 7.** Simulation results for the reference and actual motor current dq-axes components of the suggested sensorless control strategy of the proposed system for voltage dip from 300 V to 150 V.

the backward direction of the motor. A sample of the obtained results is shown in **Figures 8-10**.

It can be observed from the results that:

- The dc-link voltage is boosted and regulated at its reference value, as in case 1.

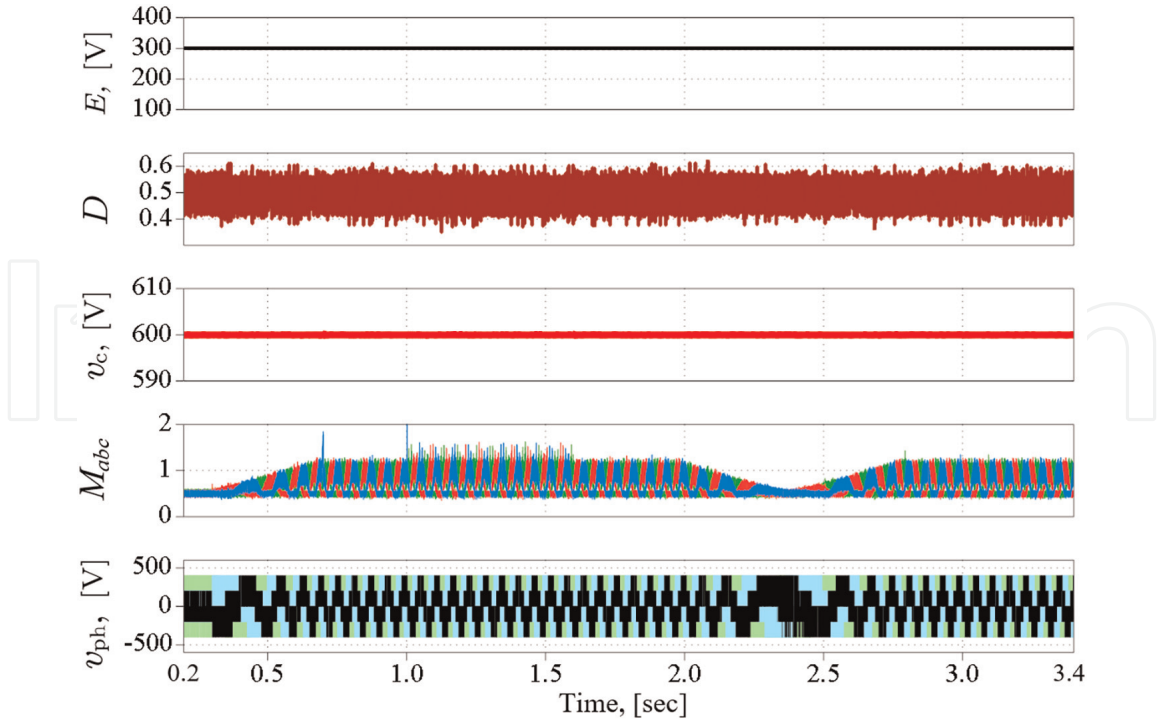


**Figure 8.** Simulation results for the supply voltage, charging duty cycle, capacitor voltage, modulating signals and motor phase voltages, respectively, of the suggested sensorless control strategy of the proposed system for a constant supply voltage of 300 V.

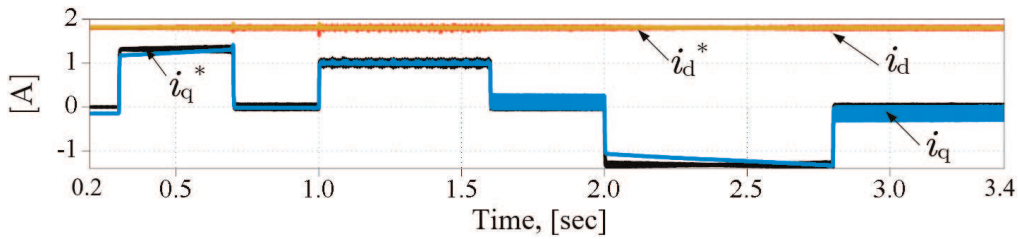


**Figure 9.** Simulation results for the reference and actual motor current dq-axes components of the suggested sensorless control strategy of the proposed system for a constant supply voltage of 300 V.

- The actual torque follows the reference torque very well. In addition, the flux and torque current components are fully decoupled.
- It can also be noted that the motor currents increase due to the loading effect at 1 sec but still have sinusoidal waveforms.
- The speed reversal transient is also examined between  $t = 2$  and  $t = 2.8$  sec.
- The responses show that the actual motor speed and the estimated speed from the proposed sensorless observer closely follow the reference value, resulting in rapid speed reversal, with torque in the limit.
- The change of phase sequence in the stator current is observed because of the change in the rotational direction.



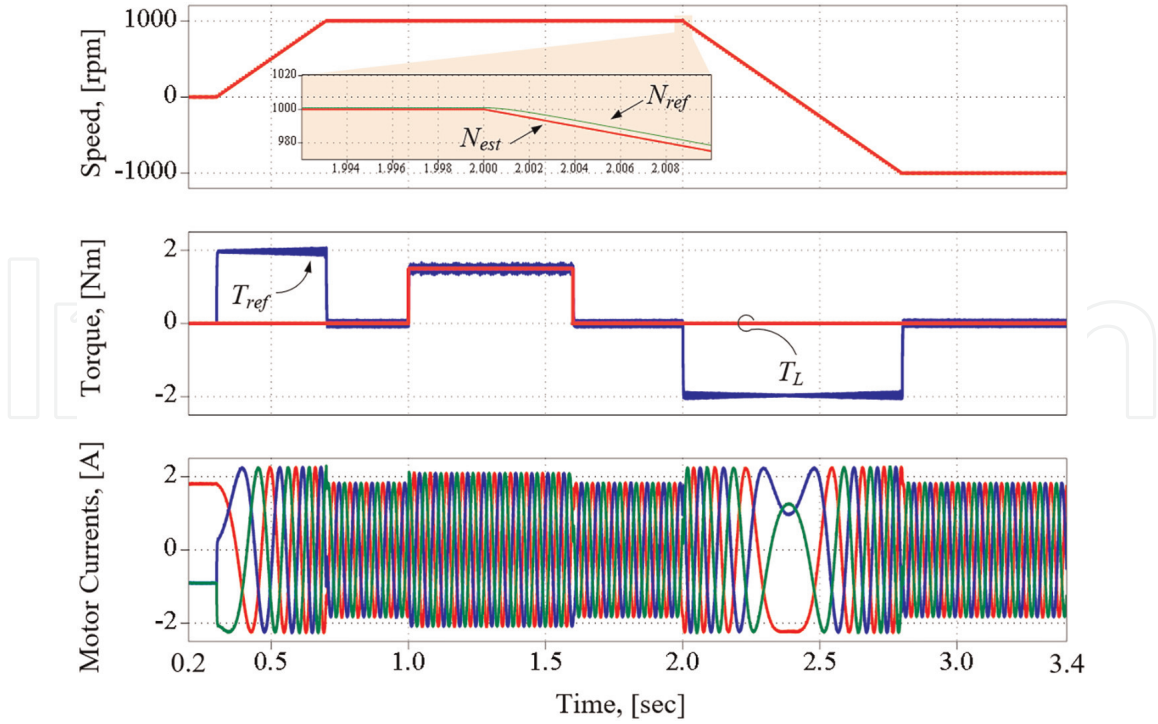


**Figure 10.** Simulation results for the reference and actual motor current  $dq$ -axes components of the suggested sensorless control strategy of the proposed system for a constant supply voltage case under different loading and speed conditions.

The above analysis and simulation results show that the proposed speed observer has been validated for indirect field-oriented control techniques with a three-phase induction motor drive based on a simplified split-source inverter.

## 5. Conclusions

In this study, a simple topology has been investigated and implemented to efficiently predict the rotor speed signal for a proposed sensorless vector control technique for an induction motor (IM) using a simplified split-source inverter configuration. The proposed observer for detecting the rotor speed has been obtained based on the principle of the phase-axis relationship of the applied machine current and indirect magnetic flux orientation control (IRFOC) method. It has been confirmed that the proposed observer procedure was simple and did not require an additional observer to detect IM rotor speed. The analysis supported by the results has confirmed the efficient performance and observability of the presented topology to predict IM speed signal with the implementation using split-source inverters compared to conventional inverters. In addition, the results have assured the controllability and robustness of the proposed observer for the sensorless control system that uses the vector control technique to drive the induction motor.

## Nomenclature

$E$	DC-supply voltage
$v_{dc}$	DC-Link Capacitor voltage



$i_L$	Supply or inductor current
$L, C$	Switching network inductance and capacitance
$D$	Charging duty cycle
$M_{abc}$	Modulating signals
$s_o - s_6$	Inverter switches
$L_{ls}, L_{lr}$	Stator and rotor windings' leakage inductances, H
$L_m$	Inductance of magnetizing, H
$i_{dr}, i_{qr}$	$dq$ -axis currents of the rotor side, A
$i_{ds}, i_{qs}$	$dq$ -axis currents of stator side, A
$r_s, r_r$	Resistances of stator and rotor windings, $\Omega$
$\theta_e$	Flux-vector electrical angle of stator side, rad.
$\lambda_{dr}, \lambda_{qr}$	$dq$ -axis flux linkages of rotor side, V.s/rad
$\lambda_{ds}, \lambda_{qs}$	$dq$ -axis flux linkages of stator side, V.s/rad.
$\lambda_r$	Flux-vector amplitude of rotor side, V.s/rad.
$\omega_e$	Stator-winding electrical angular-frequency, Hz
$\omega_f$	Reference frame mechanical angular-speed, rad./s
$\omega_{rm}$	Mechanical angular speed of the rotor, rad./s
$P$	Poles number
$T_L$	Load Torque, N.m
$B$	Coefficient friction, N.m.s/rad.
$J$	Moment of inertia, kg.m <sup>2</sup>

## Conflict of interest

The authors declare no conflict of interest.

## Author details


Sherif Dabour<sup>1,2\*</sup>, Mohamed Hussien<sup>2</sup>, Ahmed Aboushady<sup>1</sup> and Mohamed E. Farrag<sup>1</sup>

1 Glasgow Caledonian University, Glasgow, UK

2 Tanta University, Tanta, Egypt

\*Address all correspondence to: [sherif.dabour@gcu.ac.uk](mailto:sherif.dabour@gcu.ac.uk)

## IntechOpen

© 2023 The Author(s). Licensee IntechOpen. This chapter is distributed under the terms of the Creative Commons Attribution License (<http://creativecommons.org/licenses/by/3.0>), which permits unrestricted use, distribution, and reproduction in any medium, provided the original work is properly cited. 

## References

- [1] Wu B, Lang Y, Zargari N, Kouros S. *Power Conversion and Control of Wind Energy Systems*. Hoboken, New Jersey: Wiley-IEEE Press; 2011
- [2] Campanari S, Manzolini G, Iglesia FGDL. Energy analysis of electric vehicles using batteries or fuel cells through well-to-wheel driving cycle simulations. *Journal of Power Sources*. 2009;186:464-477
- [3] Zeb K et al. Indirect vector control of induction motor using adaptive sliding mode controller. In: 2016 Australian Control Conference (AuCC). Newcastle, NSW, Australia: IEEE; 2016. pp. 358-363. DOI: 10.1109/AUCC.2016.7868216
- [4] Gobinath D, Vairaperumal K, Elamcheren S. Simplified approach on feed forward vector control of induction motor with PI controller using SPWM technique. In: 2014 IEEE International Conference on Computational Intelligence and Computing Research. Coimbatore, India: IEEE; 2014. pp. 1-4. DOI: 10.1109/ICCIC.2014.7238307
- [5] Saha S, Nayak B. Sensorless vector control and selection of observer gain for speed control of indirect vector control induction motor drives. In: 2017 Second International Conference on Electrical, Computer and Communication Technologies (ICECCT). Coimbatore, India: IEEE; 2017. pp. 1-7. DOI: 10.1109/ICECCT.2017.8117987
- [6] Griva G, Ilas C, Eastham JF, Profumo F, Vranka P. High performance sensorless control of induction motor drives for industry applications. In: *Proceedings of the Power Conversion Conference - PCC '97*. Vol. 2. Nagaoka, Japan: IEEE; 1997. pp. 535-539. DOI: 10.1109/PCCON.1997.638143
- [7] Xu W, Hussien MG, Liu Y, Allam SM. Sensorless control of ship shaft stand-alone BDFIGs based on reactive-power MRAS observer. *Journal of Emerging and Selected Topics in Power Electronics*. 2021;9(2):1518-1531
- [8] W. Xu, Mohamed G. Hussien, Y. Liu, I. Rabiul, S. Allam, "Sensorless voltage control schemes for brushless doubly-fed induction generators in stand-alone and grid-connected applications," *IEEE Transactions on Energy Conversion*, vol. 35, no. 4, pp. 1781-1795, Dec. 2020
- [9] Rokhforoz P, Poshtan J. Rotor speed and resistance estimation using robust extended Kalman filter for sensorless vector control of induction motor drives. In: *The 6th Power Electronics, Drive Systems & Technologies Conference (PEDSTC 2015)*. Tehran, Iran: IEEE; 2015. pp. 304-309. DOI: 10.1109/PEDSTC.2015.7093292
- [10] Nadh G, Syamkumar U, Jayanand B. Sliding mode observer for vector control of induction motor. In: 2016 International Conference on Next Generation Intelligent Systems (ICNGIS). Kottayam, India: IEEE; 2016. pp. 1-6. DOI: 10.1109/ICNGIS.2016.7854042
- [11] Hussien MG, Hassan AE. Mathematical analysis of the small signal model for voltage-source inverter in SPMSM drive systems. In: 2019 21<sup>st</sup> International Middle East Power Systems Conference (MEPCON). Cairo, Egypt: IEEE; 2019. pp. 540-549. DOI: 10.1109/MEPCON47431.2019.9008172
- [12] Kouchih D, Hachelaf R, Boumalha N, Tadjine M, Boucherit MS. Improvement of sensorless vector controlled induction motor drives using a new algorithm for

- the rotor resistance adaptation. In: 2016 5<sup>th</sup> International Conference on Systems and Control (ICSC). Marrakesh, Morocco: IEEE; 2016. pp. 67-71. DOI: 10.1109/ICoSC.2016.7507027
- [13] Gadoue SM, Giaouris D, Finch JW. Sensorless control of induction motor drives at very low and zero speeds using neural network flux observers. *IEEE Transactions on Industrial Electronics*. 2009;**56**(8):3029-3039
- [14] Xu W, Junejo A, Liu Y, Hussien MG, Zhu J. An efficient anti-disturbance sliding-mode speed control method for PMSM drive systems. *IEEE Transactions on Power Electronics*. 2021;**36**(6): 6879-6891
- [15] Boldea I et al. Fractional kVA rating PWM converter doubly fed variable speed electric generator systems: An overview in 2020. *IEEE Access*. 2021;**9**: 117957-117968. DOI: 10.1109/ACCESS.2021.3101907
- [16] Cirrincione M, Pucci M, Cirrincione G, Capolino GA. Sensorless control of induction motor drives by new linear neural techniques. In: 2006 12<sup>th</sup> International Power Electronics and Motion Control Conference. Portoroz, Slovenia: IEEE; 2006. pp. 1820-1829. DOI: 10.1109/EPEPEMC.2006.4778670
- [17] Liu Y, Xu W, Long T, Blaabjerg F. An improved rotor speed observer for standalone brushless doubly-fed induction generator under unbalanced and nonlinear loads. *IEEE Transactions on Power Electronics*. 2020;**35**(1): 775-788
- [18] Hussien MG, Liu Y, Xu W. Robust position observer for sensorless direct voltage control of stand-alone ship shaft brushless doubly-fed induction generators. *CES Transactions on Electrical Machines and Systems*. 2019; **3**(4):363-376
- [19] Peng FZ. Z-source inverter. *IEEE Transactions on Industry Applications*. 2003;**39**(2):504-510
- [20] Caceres R, Barbi I. A boost dc-ac converter: Analysis, design, and experimentation. *IEEE Transactions on Power Electronics*. 1999;**14**(1):134-141
- [21] Abdelhakim A, Mattavelli P, Spiazzi G. Three-phase Split-source inverter (SSI): Analysis and modulation. *IEEE Transactions on Power Electronics*. 2016;**31**(11):7451-7461
- [22] Bakeer A, Dabour SM, Gowaid IA, Aboushady AA, Elgenedy MA, Farrag ME. Enhanced finite control set-model predictive control for three-phase split-source inverters. In: 2022 57<sup>th</sup> International Universities Power Engineering Conference (UPEC). Istanbul, Turkey; 2022. pp. 1-6. DOI: 10.1109/UPEC55022.2022.9917867
- [23] Abou-Hussein WM, Dabour S, Hamad MS, Rashad EM. Model predictive control based virtual synchronous generator for parallel-connected three-phase split-source converters in islanded AC microgrids. *Energy Reports*. 2023;**9**:1696-1706. DOI: 10.1016/j.egy.2022.12.075
- [24] Dabour SM, Abdel-Khalik AS, Ahmed S, Massoud A. An optimal PWM technique for dual-output nine-switch boost inverters with minimum passive component count. *IEEE Transactions on Power Electronics*. 2021;**36**(1):1065-1079. DOI: 10.1109/TPEL.2020.3001372
- [25] AbdulSalam M, Dabour SM, Rashad EM. Cascaded multilevel split-source inverters: Analysis and modulation. In: 2019 21st International Middle East Power Systems Conference (MEPCON). Cairo, Egypt; 2019. pp. 1204-1209. DOI: 10.1109/MEPCON47431.2019.9008050

[26] Dabour SM, Aboushady AA, Gowaid IA, Elgenedy MA, Farrag ME. Performance analysis and evaluation of multiphase Split-source inverters. *Energies*. 2022;**15**:8411. DOI: 10.3390/en15228411

[27] Mousa MG, Allam SM, Rashad EM. A sensorless scalar-control strategy for maximum power tracking of a grid-connected wind-driven brushless doubly-fed reluctance generator. In: *The 4<sup>th</sup> International Conference on Electric Power and Energy Conversion Systems (EPECS'15)*. UAE: American University of Sharjah; 2015. pp. 1-6

[28] Mousa MG, Allam SM, Rashad EM. Sensored and sensorless scalar-control strategy of a wind-driven BDFRG for maximum wind-power extraction. *Journal of Control and Decision*. 2018;**5** (2):1-19

[29] Hussien MG, Xu W, Liu Y, Allam SM. Rotor speed observer with extended current estimator for sensorless control of induction motor drive systems. *Energies*. 2019;**12**:3613

[30] Hussien MG, Dabour SM, Alotibi M, Omara AM, Mansour DEA. An Improved Sensorless Control of Induction Motor Drive-Based Split-Source Inverters. In: *2021 22<sup>nd</sup> International Middle East Power Systems Conference (MEPCON)*. Assiut, Egypt; 2021. pp. 378-382. DOI: 10.1109/MEPCON50283.2021.9686250

[31] Dabour SM et al. Modeling and control of single-stage quadratic-boost Split source inverters. *IEEE Access*. 2022; **10**:24162-24180. DOI: 10.1109/ACCESS.2022.3153510